Hindawi
International Journal of Aerospace Engineering
Volume 2019, Article ID 5765901, 9 pages
https://doi.org/10.1155/2019/5765901

Research Article

Analytical Predictive Guidance Algorithm Based on Single Ballistic Coefficient Switching for Mars Aerocapture

Yu-ming Peng,[1,2] **Bo Xu**,[3] **Xi Lu**,[2,4] **Bao-dong Fang**,[4] **and Heng Zhang**[2,4]

[1]*School of Astronomy and Space Science, Nanjing University, Nanjing, China*
[2]*Shanghai Institute of Satellite Engineering, Shanghai, China*
[3]*School of Aeronautics and Astronautics, Sun Yat-sen University, Shenzhen, China*
[4]*Shanghai Key Laboratory of Deep Space Exploration Technology, Shanghai, China*

Correspondence should be addressed to Yu-ming Peng; nuaapym@qq.com

Received 4 September 2018; Accepted 30 December 2018; Published 11 March 2019

Academic Editor: Franco Bernelli-Zazzera

Aerocapture can significantly reduce the velocity increment required for a planetary orbital mission and reduce the amount of propellant needed. And it may be one of the key technologies necessary for large-scale space exploration missions in the future. In this paper, the analytical solution of aerocapture based on the piecewise variable ballistic coefficient is studied around the exploration of Mars. An aerocapture analytical predictive guidance algorithm for single ballistic coefficient switching is proposed. The terminal velocity after the ballistic coefficient switching can be obtained by analytical calculation in real time. The adaptive control of the switching time of the ballistic coefficient is realized. The simulation results show that the guidance algorithm is accurate and robust, which can effectively overcome the influence of atmospheric density error, aerodynamic parameter error, and initial state uncertainty.

1. Introduction

Aerocapture is a method which uses aerodynamic drag to reduce the flight velocity of a probe and then enable it to enter the target orbit. It can significantly reduce the velocity increment required for a planetary orbital mission and reduce the amount of propellant needed. It is one of the promising technologies for large-scale space exploration missions in the future, such as a manned Mars exploration mission [1–4].

Guidance and control are significant factors affecting the success of an aerocapture. The guidance method can be divided into two categories according to the control variables: the lift-modulation method and the drag-modulation method. The first one corrects flight trajectory by lift adjustment. In this way, the probe needs to adjust the direction or magnitude of the lift like that performed by the Mars Science Laboratory [5]. The other way is based on a drag-modulation device which can change the ballistic coefficient. The drag-modulation mode can be further subdivided into the drag continuous control and the drag switching control. An analytical predictor corrector guidance algorithm based on drag continuous control is described in detail in Reference [6]. This paper focuses on the drag switching control aerocapture guidance method. In order to control the terminal velocity, the probe may need to switch the ballistic coefficient between several constant values [7], as shown in Figure 1.

A variety of aerocapture guidance algorithms have been developed for the lift modulation flight control system. Lu, Masciarelli et al., and Kozynchenko et al. have studied several analytical predictor corrector algorithms (APC) [8–12]. Rousseau proposed the energy controller algorithm (EC) [13], the numerical predictor corrector (NPC) [14, 15], and the terminal point controller (TPC) [9, 16], all of which have also been researched for a long time.

For the drag modulation flight control system, Medlock has studied the theory and applications of ballute aerocapture and proposed a dual-use ballute system for the exploration of the solar system [17]. Putnam and Braun proposed the concept of the drag modulation flight control system and analyzed the guidance performance using NPC [7]. Michael et al. has developed an Earth smallsat flight test

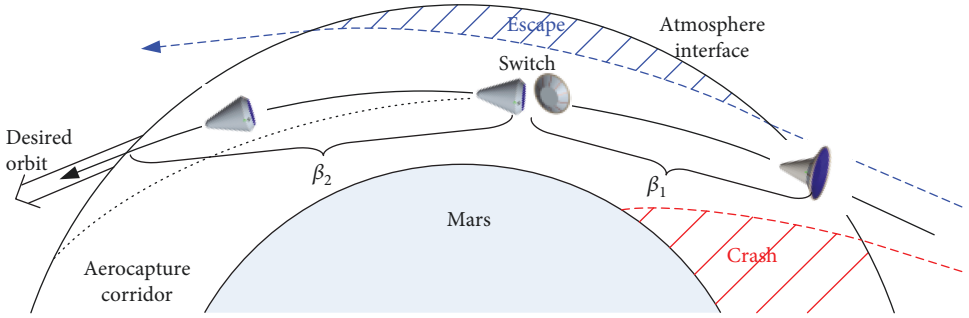

(a) One ballistic coefficient switching

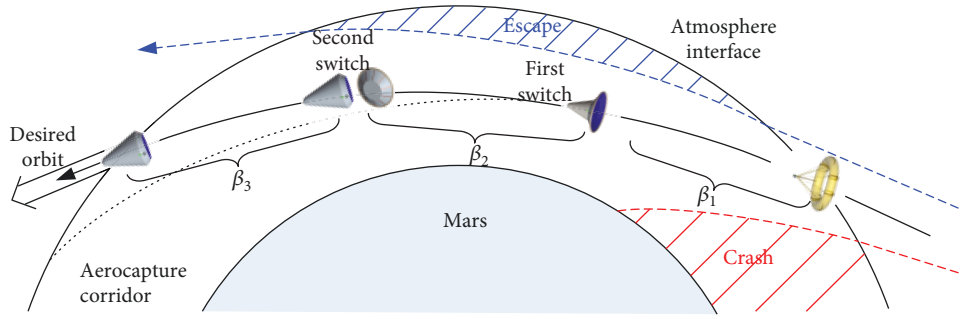

(b) Two ballistic coefficient switching

Figure 1: Aerocapture concept based on the piecewise variable ballistic coefficient.

for a Mars aerocapture [18]. Han et al. has proposed an optimal ballistic coefficient control [19]. In this paper, an analytical predictive guidance algorithm for the drag modulation flight control system is proposed. The algorithm can overcome the disadvantages of NPC and make engineering applications possible.

2. Dynamic Equation

The probe is modeled as a rigid body flying in a stationary atmosphere of a nonrotating planet which is assumed to be a sphere. The 3DOF equations of motion are given as follows [5, 6]:

$$\begin{aligned}
\dot{r} &= v \sin\gamma, \\
\dot{\theta} &= \frac{(v \cos\gamma \sin\psi)}{(r \cos\lambda)}, \\
\dot{\lambda} &= \frac{v \cos\gamma \cos\psi}{r}, \\
\dot{v} &= -D - g(r) \sin\gamma, \\
\dot{\gamma} &= \left(\frac{v}{r} - \frac{g(r)}{v}\right) \cos\gamma, \\
\dot{\psi} &= \frac{v \cos\gamma \sin\psi \tan\lambda}{r},
\end{aligned} \tag{1}$$

where r, θ, λ, v, γ, and ψ are the radius, longitude, latitude, velocity, flight path angle, and heading angle, respectively. Equation (2) defines the drag acceleration D as follows:

$$D = \frac{0.5\rho v^2}{\beta}, \quad \beta = \frac{m}{C_D S}, \tag{2}$$

where C_D is the drag coefficient, S is the reference area, m is the mass of the probe, and $\beta = m/C_D S$ is the ballistic coefficient.

A scale-height exponential density profile is used to compute the atmospheric density ρ at height h relative to the Mars surface:

$$\rho = \rho_0 e^{(-h/h_s)}, \tag{3}$$

where ρ_0 is the atmospheric density at the surface and h_s is the scale height. The gravity acceleration can be modeled with sufficient accuracy using a standard gravity model $g = \mu/r^2$, where μ is the gravitational constant.

3. Analytical Solution for Aerocapture

3.1. Ballistic Coefficient Fixed. In order to facilitate the derivation of the analytical solution for aerocapture, the following assumptions are made: the flight path angle γ is always at a small value, and the gravity acceleration is

constant with a magnitude that is equal to the value at the atmospheric interface.

$$\begin{aligned} \frac{1}{r} &\approx \frac{1}{R_{AI}}, \\ \cos\gamma &\approx 1, \\ g(r) &\approx g(R_0 + h_0), \\ g(r)\sin\gamma &\approx 0. \end{aligned} \tag{4}$$

Then, the longitudinal motion equation becomes:

$$\begin{aligned} \dot{r} &= v\sin\gamma, \\ \dot{v} &= \frac{-0.5\rho v^2 C_D S}{m}, \\ \dot{\gamma} &= \left(\frac{v}{R_{AI}} - \frac{g}{v}\right). \end{aligned} \tag{5}$$

We define the following dimensionless variables:

$$\begin{aligned} Z &= \frac{\sqrt{R_{AI}h_s}\rho C_D S}{m}, \\ \phi &= -\sqrt{\frac{R_{AI}}{h_s}}\sin\gamma, \\ x &= \ln\left(\frac{v_0^2}{v^2}\right), \\ \alpha &= \frac{gR_{AI}}{v_0^2}, \end{aligned} \tag{6}$$

where R_{AI} is the radius at the interface of the atmosphere and v_0 is the initial entry velocity. Then, the above longitudinal motion equation can be transformed into:

$$\begin{aligned} \frac{dZ}{dx} &= \phi, \\ \frac{d\phi}{dx} &= \frac{(\alpha e^x - 1)}{Z}. \end{aligned} \tag{7}$$

With the initial conditions,

$$\begin{aligned} Z(x=0) &= \frac{\sqrt{R_{AI}h_s}\rho_{AI}C_D S}{m} = \varepsilon, \\ \phi(x=0) &= -\sqrt{\frac{R_{AI}}{h_s}}\sin\gamma_0 = c. \end{aligned} \tag{8}$$

The previous equation is the classical Yaroshevskii equation. According to Reference [19], we shall use the Poincare method by artificially inserting a small parameter ε.

We define the following variables:

$$\begin{aligned} y &= \frac{Z}{\varepsilon}, \\ \tau &= \frac{x}{\varepsilon}. \end{aligned} \tag{9}$$

Then,

$$\begin{aligned} \frac{dy}{d\tau} &= \phi, \\ \frac{d\phi}{d\tau} &= \frac{(\alpha e^{\varepsilon\tau} - 1)}{y}. \end{aligned} \tag{10}$$

With the initial conditions,

$$\begin{aligned} y(\tau=0) &= 1, \\ \phi(\tau=0) &= c. \end{aligned} \tag{11}$$

Then, the zero-order solution of the aerocapture dynamic equation can be expressed as the following form:

$$\frac{dy}{d\phi} = -\frac{y\phi}{(1-\alpha)}. \tag{12}$$

It can be obtained by integrating the following:

$$\begin{aligned} y &= \exp\left(\frac{(c^2 - \phi^2)}{\delta}\right), \\ \tau &= \sqrt{\frac{\pi}{\delta}}\exp\left(\frac{c^2}{\delta}\right)\left(\operatorname{erf}\left(\frac{c}{\sqrt{\delta}}\right) - \operatorname{erf}\left(\frac{\phi}{\sqrt{\delta}}\right)\right), \end{aligned} \tag{13}$$

where $\delta = 2(1-\alpha)$ and $\operatorname{erf}(x) = 2\pi^{-1/2}\int_0^x e^{-t^2}dt$.

Figure 2 shows the accuracy of the zero-order solution for different initial flight path angles.

It can be found that when the initial flight path angle γ_0 is less than 8.5 deg, the error of the terminal velocity v_f is maintained at a low level of only 20 m/s. However, if the initial flight path angle exceeds this threshold, the terminal velocity shows a large deviation. The specific reason has been analyzed in Reference [19], and the correction algorithm is given as follows:

$$x + \alpha(1 - e^x) = \frac{\varepsilon}{2}\sqrt{\pi\delta}\exp\left(\frac{c^2}{\delta}\right)\left(\operatorname{erf}\left(\frac{c}{\sqrt{\delta}}\right) - \operatorname{erf}\left(\frac{\phi}{\sqrt{\delta}}\right)\right). \tag{14}$$

The corrected analytical solution is shown in Figure 3. It can be seen that the algorithm can effectively reduce the terminal velocity error.

3.2. Ballistic Coefficient Switching. Ideally, the probe can achieve aerocapture with a constant ballistic coefficient if there are no initial errors and parameter errors. However,

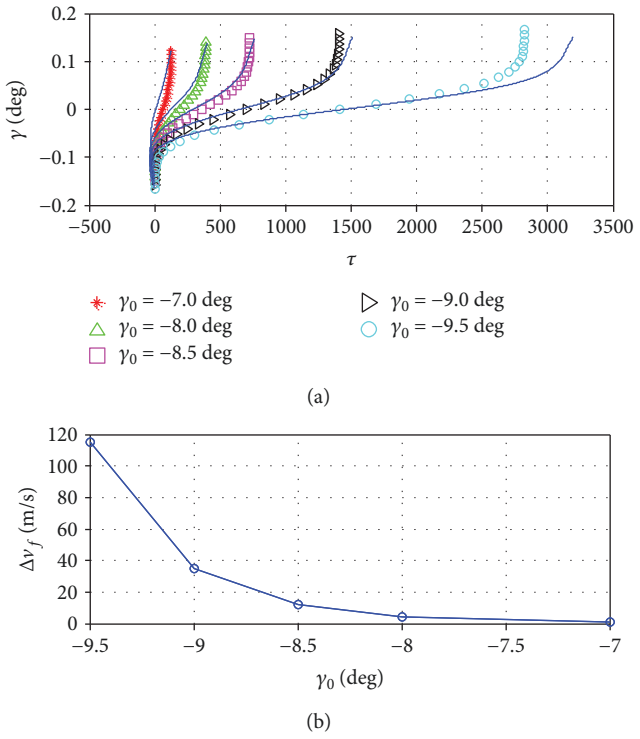

Figure 2: The zero-order solution for aerocapture.

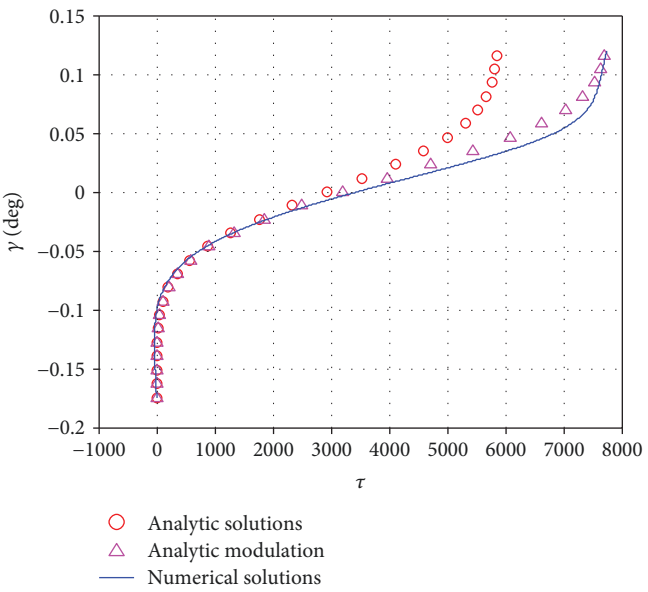

Figure 3: The corrected analytical solution vs. the numerical solution when $\gamma_0 = -10^\circ$.

the error is actually difficult to eliminate, so it is necessary for the probe to have an ability to adjust and control the trajectory. Then, the ballistic coefficient switching is a simple and effective control method. In the case where the number of ballistic coefficient switching is limited, the dynamic equation can be described in the form of a piecewise function. The following is an example of only one ballistic coefficient switching, from which the characteristics of the analytical solution can be obtained.

First, we define the state at the moment of ballistic coefficient switching r_s, v_s, and γ_s. They correspond to y_s, τ_s, and ϕ_s, respectively. Subscript "1" is used to indicate the parameters and state before ballistic coefficient switching. Therefore, the parameters before switching are shown as follows:

$$\begin{aligned}
\varepsilon_1 &= \frac{\sqrt{R_{AI} h_s}\rho_{AI}}{\beta_1}, \\
c_1 &= -\sqrt{\frac{R_{AI}}{h_s}} \sin\gamma_0, \\
\alpha_1 &= \frac{gR_{AI}}{v_0^2}, \\
\delta_1 &= 2(1-\alpha_1).
\end{aligned} \tag{15}$$

Similarly, subscript "2" is used to indicate the parameters and state after ballistic coefficient switching:

$$\begin{aligned}
\varepsilon_2 &= \frac{\sqrt{R_{AI} h_s}\rho_{AI}}{\beta_2}, \\
c_2 &= -\sqrt{\frac{R_{AI}}{h_s}} \sin\gamma_s, \\
\alpha_2 &= \frac{gR_{AI}}{v_s^2}, \\
\delta_2 &= 2(1-\alpha_2).
\end{aligned} \tag{16}$$

Then, before the ballistic coefficient is switched, $\phi \le \phi_s$. The analytical solutions are the same as the constant ballistic coefficient.

$$\begin{aligned}
x_1 + \alpha_1(1 - e^{x_1}) &= \frac{\varepsilon_1}{2}\sqrt{\pi\delta_1}\exp\left(\frac{c_1^2}{\delta_1}\right) \\
&\quad \cdot \left(\operatorname{erf}\left(\frac{c_1}{\sqrt{\delta_1}}\right) - \operatorname{erf}\left(\frac{\phi}{\sqrt{\delta_1}}\right)\right), \\
y_1 &= \exp\left(\frac{(c_1^2 - \phi^2)}{\delta_1}\right), \\
\tau_1 &= \frac{x_1}{\varepsilon_1}.
\end{aligned} \tag{17}$$

However, it is impossible to directly solve y by equation (13) because of the ballistic coefficient switching when $\phi > \phi_s$.

Therefore, according to the definition of the zero-order solution, the two sides of equation (12) are integrated as follows:

$$\int_1^{y_2} \frac{1}{y} dy = -\int_{c_1}^{\phi_s} \frac{1}{1-\alpha_1} \phi d\phi - \int_{\phi_s}^{\phi} \frac{1}{1-\alpha_2} \phi d\phi. \tag{18}$$

After a series of simplifications, the analytical solution after ballistic coefficient switching can be obtained:

$$\begin{aligned} x_2 + \alpha_2(1-e^{x_2}) &= \frac{\varepsilon_2}{2}\sqrt{\pi\delta_1}\exp\left(\frac{c_1^2}{\delta_1}\right) \\ &\quad \cdot \left(\operatorname{erf}\left(\frac{c_2}{\sqrt{\delta_2}}\right) - \operatorname{erf}\left(\frac{\phi}{\sqrt{\delta_2}}\right)\right), \\ y_2 &= \exp\left(\ln(y_s) + \frac{\left(c_2^2 - \phi^2\right)}{\delta_2}\right), \\ \tau_2 &= \frac{x_s}{\varepsilon_1} + \frac{x_2}{\varepsilon_2}. \end{aligned} \tag{19}$$

Similarly, when ballistic coefficient switching occurs two or more times, the above derivation process is repeated to get a new analytical solution:

$$\begin{aligned} x_3 + \alpha_3(1-e^{x_3}) &= \frac{\varepsilon_3}{2}\sqrt{\pi\delta_1}\exp\left(\frac{c_1^2}{\delta_1}\right) \\ &\quad \cdot \left(\operatorname{erf}\left(\frac{c_3}{\sqrt{\delta_3}}\right) - \operatorname{erf}\left(\frac{\phi}{\sqrt{\delta_3}}\right)\right), \\ y_3 &= \exp\left(\ln(y_{s1}) + \ln(y_{s2}) + \frac{\left(c_3^2 - \phi^2\right)}{\delta_3}\right), \\ \tau_3 &= \frac{x_{s1}}{\varepsilon_1} + \frac{x_{s2}}{\varepsilon_2} + \frac{x_3}{\varepsilon_3}, \end{aligned} \tag{20}$$

where subscript "3" in equation (20) represents the parameter and state after the second ballistic coefficient switching. In order to intuitively understand the accuracy of the analytical solution, the numerical solution is used for comparison as shown in Figures 4 and 5. It can be seen that the analytical solution and the numerical solution show good consistency, which demonstrates the effectiveness of the analytical algorithm. It should be noted that the initial state after the ballistic coefficient switching is obtained by real-time measurement, rather than from the analytical solution, so that the accumulation of algorithm errors can be avoided.

4. Guidance Law and Simulation

The design of the guidance law is relatively simple in the case where the trajectory and the terminal state of the probe can be predicted. Since the probe is not affected by aerodynamic drag after flying out of the atmosphere, the velocity at the atmosphere's interface directly determines the final capture orbit. Therefore, the basic guidance strategy is to calculate the analytical solution in real time based on the current state and the ballistic coefficient after switching. It is then determined whether to switch the ballistic coefficient by comparing the predicted terminal velocity to the desired terminal velocity.

4.1. APC Algorithm for Ballistic Coefficient Switching. By definition, the terminal state y_f meets the following:

$$y_f = \exp\left(\ln(y_s) + \frac{\left(c_2^2 - \phi_f^2\right)}{\delta_2}\right) = 1. \tag{21}$$

Further, the following equation can be obtained:

$$\phi_f = -\sqrt{\delta_2 \ln(y_s) + c_2^2}. \tag{22}$$

Substituting equation (22) into equation (19), we have

$$\begin{aligned} x_f + \alpha_2(1-e^{x_f}) &= \frac{\varepsilon_2}{2}\sqrt{\pi\delta_1}\exp\left(\frac{c_1^2}{\delta_1}\right) \\ &\quad \cdot \left(\operatorname{erf}\left(\frac{c_2}{\sqrt{\delta_2}}\right) - \operatorname{erf}\left(\frac{\phi_f}{\sqrt{\delta_2}}\right)\right). \end{aligned} \tag{23}$$

By solving the above transcendental equation about x_f, we can get

$$\tau_f = \frac{x_s}{\varepsilon_1} + \frac{x_f}{\varepsilon_2}. \tag{24}$$

Therefore, the terminal velocity can be predicted based on the current state:

$$v_{f\text{predict}} = v_s \exp\left(\frac{\ln\left(v_0^2/v_s^2\right)\varepsilon_2}{2\varepsilon_1} - \frac{\varepsilon_2\tau_f}{2}\right). \tag{25}$$

When $\beta_1 < \beta_2$, $v_{f\text{predict}}$ is monotonically increasing with time, and it satisfies the following inequality:

$$v_{\text{circle}} < v_{f\text{predict}} < v_{f2}, \tag{26}$$

where v_{circle} is the velocity of the circular orbit, and v_{f2} is the terminal velocity when the probe flies with constant ballistic coefficient β_2.

When $\beta_1 > \beta_2$, $v_{f\text{predict}}$ is monotonically decreasing with time, and it satisfies the following inequality:

$$v_{f1} < v_{f\text{predict}} < v_{f2}, \tag{27}$$

where v_{f1} is the terminal velocity when the probe flies with constant ballistic coefficient β_1.

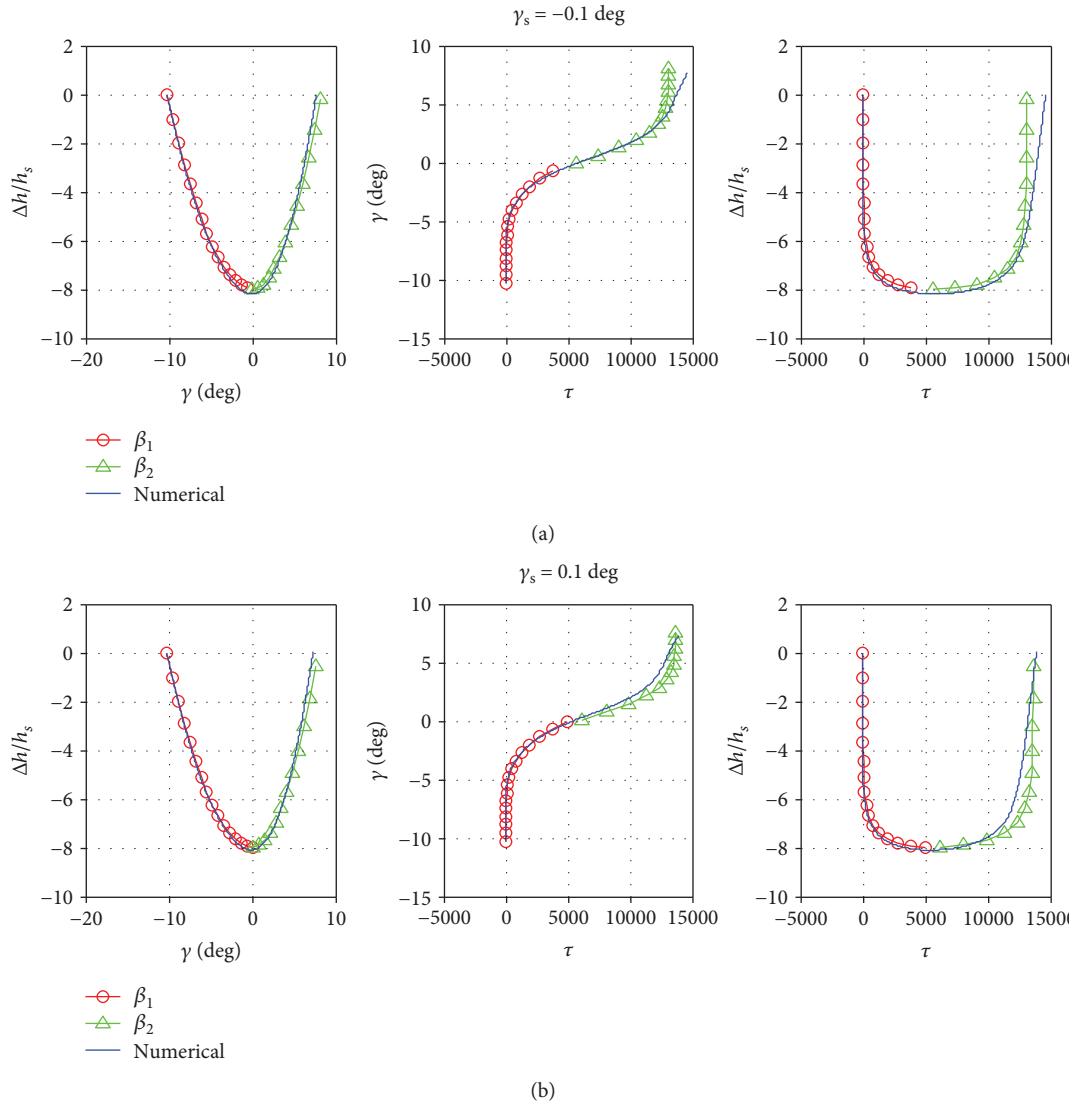

Figure 4: Analytical solution for single ballistic coefficient switching.

Obviously, the desired terminal velocity $v_{f\text{desired}}$ must be within the variable range of $v_{f\text{predict}}$. It is the moment of ballistic coefficient switching when $v_{f\text{predict}} = v_{f\text{desired}}$.

4.2. Simulation Condition and Parameters. The numerical simulation is carried out for the human exploration of Mars, which is used to verify the effectiveness of the guidance algorithm. First, the simulation parameters and initial values need to be given. The probe configuration is similar to the human Mars lander mentioned in Reference [20]; however, the separation device for an inflatable aerodynamic decelerator is added, and the Mars descent module (MDM) is removed, so the total mass was reduced to 45 metric tons. The parameters are shown in Table 1. The value of the ballistic coefficient comes from Reference [6], and the drag coefficients are calculated by other parameters.

The initial entry conditions are borrowed from Reference [6]. It should be noted that the desired aerocapture orbit is different from the Mars parking orbit. After aerocapture, the probe still needs several maneuvers to enter the Mars parking orbit. Considering the uncertain factors during aerocapture, a capture orbit with an apoapsis height of 3000 km is selected, which allows more margin. The initial conditions and desired orbit are shown in Table 2.

Since the entire aerocapture process lasts only 200~300 s, the effects of the rotation and gravitational perturbation of Mars are negligible. The gravitational constant μ is taken as $4.2828 \times 10^4\ \text{km}^3/\text{s}^2$, and Mars radius R_0 is taken as 3397 km. The validity of the atmospheric model directly affects the effectiveness of the guidance algorithm performance evaluation. A simplified atmospheric model from Reference [6] was used, where random error with height variation is added to the exponential atmospheric density model.

4.3. Simulation Results and Analysis. Figure 6 shows the distribution of the periapsis and apoapsis altitude of the terminal orbit with different ballistic coefficient ratios. It can be found that the distribution error of the periapsis

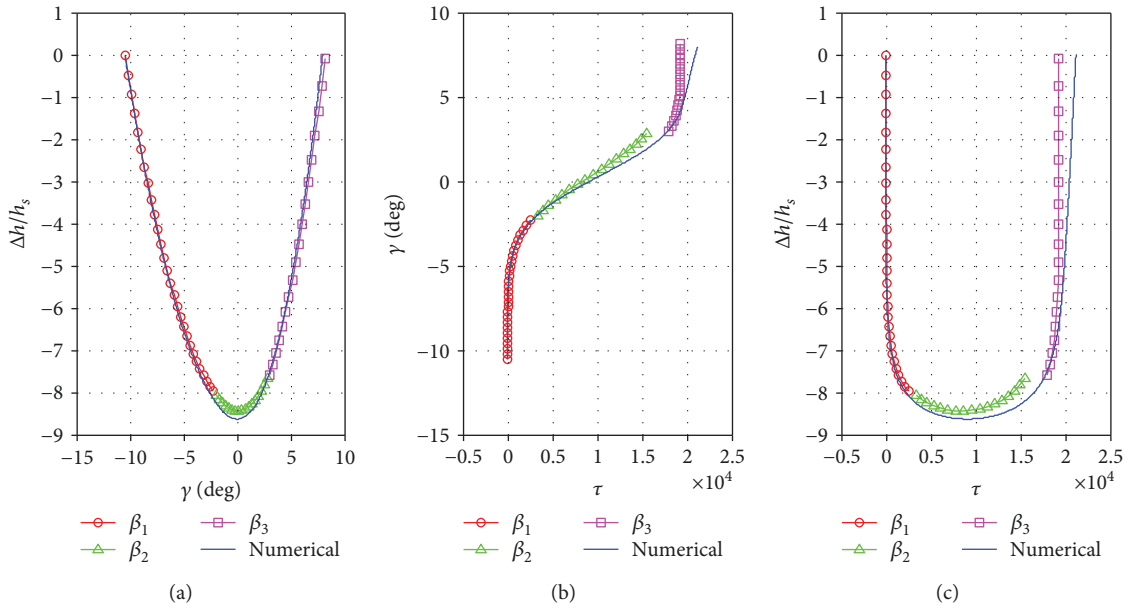

Figure 5: Analytical solution for double ballistic coefficient switching.

Table 1: Probe parameters for Monte Carlo simulation [6, 20].

Parameters	Nominal	Error	Distribution type
Initial mass m_0	45,000 kg	—	—
Deployed diameter D_1	18.8 m	—	—
Folding diameter D_2	7 m	—	—
Drag coefficient C_{D1}	1.62	±10%	Gaussian
Drag coefficient C_{D2}	1.46	±10%	Gaussian
Ballistic coefficient β_1	100 kg/m^2	±10%	Gaussian
Ballistic coefficient β_2	800 kg/m^2	±10%	Gaussian

Table 2: Initial state and desired orbit for Monte Carlo simulation [6].

Parameters	Nominal	Error	Distribution type
Initial velocity v_0	6.5 km/s	±20 m/s	Gaussian
Initial radius r_0	3522 km	±1 km	Gaussian
Initial FPA γ_0	-11 deg	±0.1°	Gaussian
Initial longitude θ_0	5 deg, E	±0.05°	Gaussian
Initial latitude λ_0	5 deg, N	±0.05°	Gaussian
Initial heading angle ψ_0	20 deg	±0.05°	Gaussian
Periapsis altitude h_p	35 km	—	—
Apoapsis height h_a	3000 km	—	—
Atmosphere interface $h_{\text{interface}}$	125 km	—	—

altitude is less than 8 km, and it gradually decreases as the ballistic coefficient ratio increases; it is reduced to 5 km when $\beta_2/\beta_1 = 8$. However, the distribution error of the apoapsis altitude is relatively large and inversely proportional to the ballistic coefficient ratio, and it is asymmetric. When $\beta_2/\beta_1 = 4$, the apoapsis altitude is mostly distributed in the range of 3200~3700 km, and this interval becomes 2800~3200 km when $\beta_2/\beta_1 = 6$. However, when $\beta_2/\beta_1 = 8$, the apoapsis altitude decreased to 2800~3000 km. The same phenomenon can be found in Figure 7, and it is mainly caused by the approximation error of the analytical solution of aerocapture.

As the ballistic coefficient ratio increases, the distribution error of the terminal velocity gradually decreases as shown in Figure 8. However, the terminal velocity error does not decrease indefinitely, and it is maintained at a relatively stable value when the ballistic coefficient ratio exceeds 8. According to the previous derivation, the terminal velocity error mainly includes two parts, one is the guidance algorithm error caused by the analytical solution approximation error, and the other part is caused by the parametric error such as aerodynamic parameters and atmospheric model. After the ballistic coefficient is switched, the probe loses the orbital control capability. The deviation will gradually accumulate and be reflected in the final capture orbit. When the ballistic coefficient ratio is increased to a certain value, the drag becomes smaller after the ballistic coefficient switched, and the terminal velocity error also decreases. When the ballistic coefficient β_2 is infinite, the terminal speed error only has the guidance error. If the ballistic coefficient β_2 is infinite, then the terminal velocity is not affected by aerodynamic parameters and atmospheric model errors.

5. Conclusion

In this paper, the analytical solution of aerocapture based on the piecewise variable ballistic coefficient is studied around the exploration of Mars. An aerocapture analytical predictive

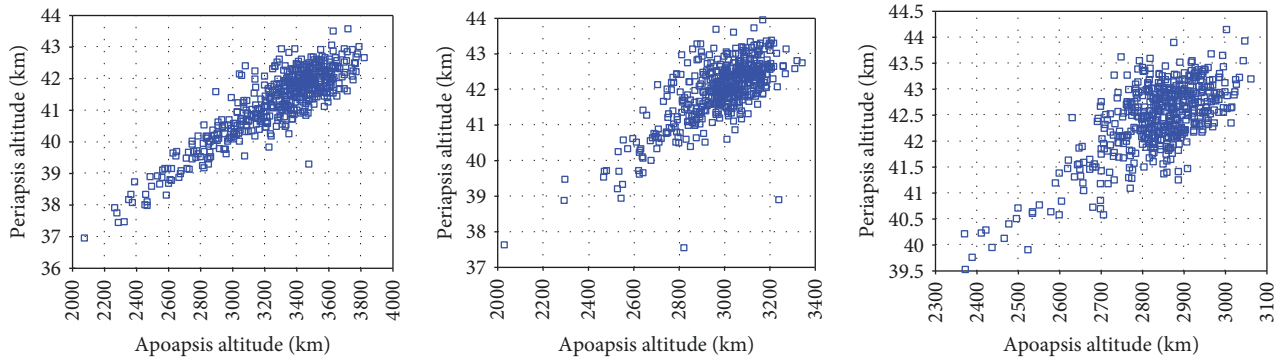

(a) $\beta_2/\beta_1 = 4$ (b) $\beta_2/\beta_1 = 6$ (c) $\beta_2/\beta_1 = 8$

FIGURE 6: The distribution of periapsis and apoapsis of the captured orbit.

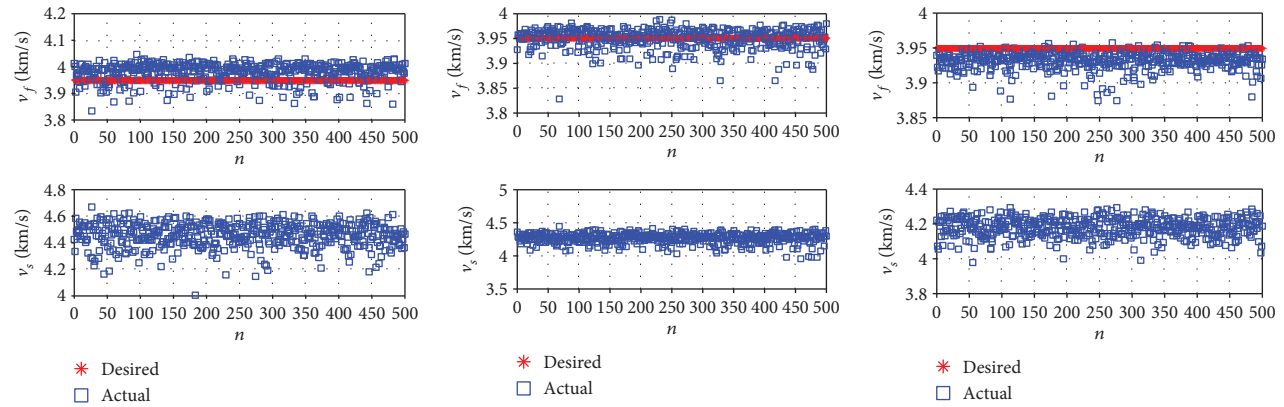

(a) $\beta_2/\beta_1 = 4$ (b) $\beta_2/\beta_1 = 6$ (c) $\beta_2/\beta_1 = 8$

FIGURE 7: The distribution of terminal velocity and switching velocity.

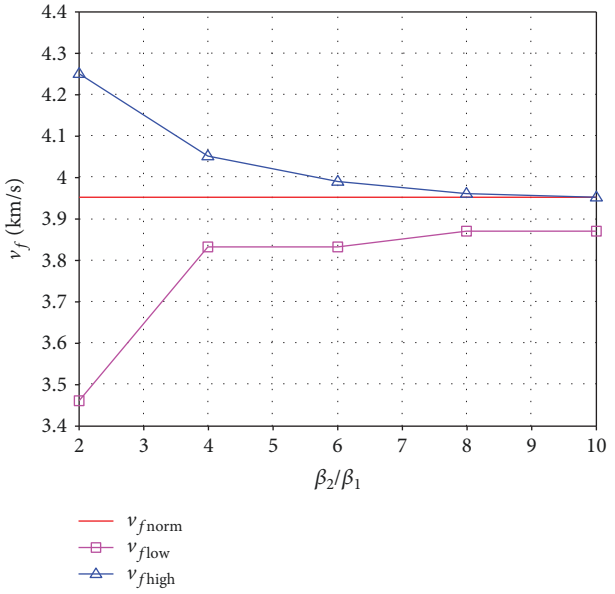

FIGURE 8: The boundary of terminal velocity.

guidance algorithm for single switching of ballistic coefficients is proposed. The terminal velocity after the ballistic coefficient switching can be obtained by analytical calculation in real time. The adaptive control of the switching time of the ballistic coefficient is realized. The simulation results show that the guidance algorithm is accurate and robust, which can effectively overcome the influence of atmospheric density error, aerodynamic parameter error, and initial state uncertainty.

Data Availability

Previously reported analytical solution analysis data were used to support this study and are available at "Second-Order Analytic Solutions for Aerocapture and Ballistic Fly-Through Trajectories," The Journal of the Astronautical Sciences, Vol. 32, No. 4, Oct.–Dec. 1984. These prior studies are cited at relevant places within the text as references [19]. The initial state and parameters for Monte Carlo simulation used to support the findings of this study are included within the article. The atmospheric model data used to support the findings of this study are included within the supplementary information file "Atmospheric model.docx" (available here).

The simulation result data used to support the findings of this study are included within the supplementary information file "simulation result.docx".

Conflicts of Interest

All the authors do not have any possible conflicts of interest.

Acknowledgments

This study was supported by the National Basic Research Program 973 of China (2015CB857100), The Base of National Defense Scientific Research Fund (no. 2016110C019), the National Natural Science Foundation of China (no. 11603011), and the Civil Aerospace Preresearch Program (no. D030106)

Supplementary Materials

The supplementary materials include two files. One of them is the Mars atmospheric density model used in the paper. It is based on an exponential model, and the time-varying characteristics are determined by 6 random variation parameters. The file is the source code based on MATLAB. The second file is the simulation result of the paper. In the text, only part of the simulation results are shown. In order to maintain the integrity of the article, the complete simulation results are given in the file, including various cases where the ballistic coefficient ratio is from 2 to 10. *(Supplementary Materials)*

References

[1] J. M. Salotti, "Robust, affordable, semi-direct Mars mission," *Acta Astronautica*, vol. 127, pp. 235–248, 2016.

[2] J. L. Hall, M. A. Noca, and R. W. Bailey, "Cost-benefit analysis of the aerocapture mission set," *Journal of Spacecraft and Rockets*, vol. 42, no. 2, pp. 309–320, 2005.

[3] P. L. K Webb and A. M. D. Cianciolo, "Aerocapture guidance for human Mars missions," in *AIAA Guidance, Navigation, and Control Conference*, pp. 1–23, Grapevine, TX, USA, January 2017.

[4] J. M. Salotti and E. Suhir, "Manned missions to Mars: minimizing risks of failure," *Acta Astronautica*, vol. 93, pp. 148–161, 2014.

[5] D. W. Way, R. W. Powell, A. Chen et al., "Mars Science Laboratory: entry, descent and landing system performance," in *2007 IEEE Aerospace Conference*, pp. 1–19, Big Sky, MT, USA, March 2007.

[6] Y. M. Peng, B. Xu, B. D. Fang, and H. L. Lei, "Analytical predictor-corrector guidance algorithm based on drag modulation flight control system for Mars aerocapture," *International Journal of Aerospace Engineering*, vol. 2018, Article ID 5907981, 12 pages, 2018.

[7] Z. R. Putnam and R. D. Braun, "Drag-modulation flight control system options for planetary aerocapture," *Journal of Spacecraft and Rockets*, vol. 51, no. 1, pp. 139–150, 2014.

[8] P. Lu, "Entry guidance: a unified method," *Journal of Guidance, Control, and Dynamics*, vol. 37, no. 3, pp. 713–728, 2014.

[9] J. Masciarelli, S. Rousseau, H. Fraysse, and E. Perot, "An analytic aerocapture guidance algorithm for the Mars sample return orbiter," in *Atmospheric Flight Mechanics Conference*, pp. 525–529, Denver, CO, USA, August 2000.

[10] E. Perot, H. Fraysse, S. Rousseau, and J. Berges, "Comparison of an analytic predictor-corrector and a terminal point controller for the Mars sample return aerocapture," in *Association A'eronautique et Astronautique de France, Paper AAAF*, pp. 14–67, March 2001.

[11] J. F. Hamel and J. Lafontaine, "Improvement to the analytical predictor-corrector guidance algorithm applied to Mars aerocapture," *Journal of Guidance, Control, and Dynamics*, vol. 29, no. 4, pp. 1019–1022, 2006.

[12] A. Kozynchenko, "Development of optimal and robust predictive guidance technique for Mars aerocapture," *Aerospace Science and Technology*, vol. 30, no. 1, pp. 150–162, 2013.

[13] S. Rousseau, "An energy controller aerocapture guidance algorithm for the Mars sample return orbiter," in *Proceedings of the 11th Annual AAS/AIAA Space Flight Mechanics Meeting*, pp. 67–83, Santa Barbara, CA, USA, Febuary 2001.

[14] A. M. Daniel, P. Lu, and G. F. Mendeck, "Application of a fully numerical guidance to Mars aerocapture," in *AIAA Guidance, Navigation, and Control Conference*, pp. 1–8, Grapevine, TX, USA, 2017.

[15] J. Berges, S. Rousseau, and E. Perot, "A numerical predictor-corrector guidance algorithm for the Mars sample return aerocapture," in *Association A'eronautique et Astronautique de France*, pp. 14–66, Paper AAAF, 2001.

[16] T. Ro and E. Queen, "Study of martian aerocapture terminal point guidance," in *23rd Atmospheric Flight Mechanics Conference*, pp. 1–5, Boston, MA, USA, August 1998.

[17] K. L. G. Medlock, *Theory and Applications of Ballute Aerocapture and Dual-Use Ballute Systems for Exploration of the Solar System*, Purdue University, 2009.

[18] S. W. Michael, A. W. Bryce, and T. Anirudh, "Development of an Earth smallsat flight test to demonstrate viability of Mars aerocapture," in *55th AIAA Aerospace Sciences Meeting*, pp. 1–16, Grapevine, TX, USA, January 2017.

[19] H. W. Han, D. Qiao, and H. B. Chen, "Optimal ballistic coefficient control for Mars aerocapture," in *2016 IEEE Chinese Guidance, Navigation and Control Conference (CGNCC)*, pp. 45–58, Nanjing, China, August 2016.

[20] T. Polsgrove, J. Chapman, S. Sutherlin et al., "Human Mars lander design for NASA's evolvable Mars campaign," in *2016 IEEE Aerospace Conference*, pp. 6–13, Big Sky, MT, USA, March 2016.